



HAL
open science

Quantification and uncertainty analysis of a structural monitoring device: detection of chloride in concrete using DC electrical resistivity measurement

Yann Lecieux, Franck Schoefs, Stéphanie Bonnet, Trystan Lecieux, Sérgio Palma Lopes

► To cite this version:

Yann Lecieux, Franck Schoefs, Stéphanie Bonnet, Trystan Lecieux, Sérgio Palma Lopes. Quantification and uncertainty analysis of a structural monitoring device: detection of chloride in concrete using DC electrical resistivity measurement. *Nondestructive Testing and Evaluation*, 2015, 30 (3), pp.216-232. 10.1080/10589759.2015.1029476 . hal-01404057

HAL Id: hal-01404057

<https://hal.science/hal-01404057>

Submitted on 1 Feb 2024

HAL is a multi-disciplinary open access archive for the deposit and dissemination of scientific research documents, whether they are published or not. The documents may come from teaching and research institutions in France or abroad, or from public or private research centers.

L'archive ouverte pluridisciplinaire **HAL**, est destinée au dépôt et à la diffusion de documents scientifiques de niveau recherche, publiés ou non, émanant des établissements d'enseignement et de recherche français ou étrangers, des laboratoires publics ou privés.

Quantification and uncertainty analysis of a structural monitoring device: detection of chloride in concrete using DC electrical resistivity measurement

Yann Lecieux^{a*}, Franck Schoefs^a, Stéphanie Bonnet^a, Trystan Lecieux^a and Sérgio Palma Lopes^b

^aGeM, CNRS UMR 6082, UNAM, Université de Nantes, 2 rue de la Houssinière, 44322 Nantes, France

^bL'UNAM-IFSTTAR, Route de Bouaye, 44340 Bouguenais, France

In this work, we seek to assess and optimise the performance of an integrated chloride detection sensor based on the DC electrical resistivity measurement. We specifically seek to evaluate the detection threshold of chlorides. The main problem of the resistivity measurements in concrete is the dispersion of results mainly linked to the material heterogeneity and electrical contact limitations. To take into account the uncertainty of the measurement, we used a measurement device and sensors based on Geoelectrical Imaging methods. It gives richer information than the one delivered by conventional resistivity measurement sensors. Thus, it allows the use of statistical analysis and quality assessment methods. Before performing tests in concrete, we worked in a medium of known and homogenous resistivity in order to assess and optimise the performances of the acquisition system. Then we performed tests on concrete specimens containing different contents of chloride ions. Performance assessment of the resistivity probe is based on an analysis of receiver operating characteristic curves and the detection threshold of chlorides is calculated using the $\alpha\delta$ method.

Keywords: embedded sensors; chloride; concrete; resistivity; uncertainty analysis

1. Introduction

Corrosion of steel reinforcements is the main cause of deterioration of reinforced concrete structures in the marine environment. It is mainly due to the penetration of chloride ions in the concrete porosity. The chlorides cause the pitting of the reinforcements. The severity of the pathology increases with the content of NaCl ions.

It is not easy to measure directly the initiation of corrosion. Consequently, we often prefer to observe a phenomenon linked to the corrosion. To this end, several methods are available.[1] In the context of this article, we focus on the DC electrical resistivity measurement. Indeed, the main factors affecting the resistivity of a porous medium include porosity, water content and chloride content.[2] These parameters are determinant in the start of the corrosion process. The study of the resistivity of concrete is thus a good indicator of the durability of the structure.[3–5] Many experimental devices of resistivity measurements exist, in particular multi-rings resistivity cells or electrode probes.[3,4,6,7]

The main problem of the resistivity measurements in concrete is the dispersion of results. The coefficient of variation (CoV) of the resistivity commonly takes values from 10% to 25% in different specimens of the same concrete under similar conditions

*Corresponding author. Email: yann.lecieux@univ-nantes.fr

(temperature, humidity).[3,8–10] This dispersion has various origins: the heterogeneity of the material, the quality of the electrical contacts and the noise measurement of the acquisition system itself. With such CoV, the uncertainty of the resistivity measurement cannot be neglected and has been shown to play a major role in maintenance optimisation. [11] Statistical analysis and quality assessment methods are used to take into account these uncertainties for quantification. These methods require a large number of measurement points to be applied. Therefore, in this work, we employed a resistivity sensor which is an evolution of the one proposed in [7]. This sensor is directly inspired by the technique of soil resistivity measurements based on electrical tomography used in Geophysics. It gives richer information than the one delivered by conventional devices (such as four electrodes Wenner probes). In addition, this sensor can be embedded in concrete which is an important point for a future *in-situ* integration and spatial variability assessment.

The goal of this project is to assess and optimise the performances of an integrated resistivity sensor based on Geoelectrical Imaging methods. In this way, we have performed tests in a controlled environment. We specifically seek to evaluate the detection threshold of chlorides by carrying out tests on concrete specimens containing different concentrations of these ions.

We assume that except the chloride content, several factors affecting the resistivity measure are fixed: specimens of the same chemical composition with temperature and humidity control. Thus, variations come from material variability, heterogeneity and measurement device including the probe-concrete interface. Performance evaluation of the resistivity probe is based on an analysis of receiver operating characteristic (ROC) curves and the detection threshold of chlorides is calculated using the $\alpha\delta$ method.[12]

The sensor operating principle is explained in Section 2. In the next section we give the performances objectives of the sensor. In Section 4 we present the results on tests performed in a material of known resistivity. Then in Section 5 we give the results of the experiments carried out on concrete and the data analysis allows calculation of the detection threshold of chlorides.

2. Resistivity measurement using a multi-electrode Wenner probe

The sensor used in this study is directly inspired by the technique of soil resistivity measurements based on electrical tomography and used in Near Surface Geophysics.[13] This technique consists of successively measuring the electrical potential drops between different pairs of electrodes on a line.

2.1 Physical principle of the resistivity measurement

We consider the diffusion in a homogenous medium, of which the electrical resistivity is noted ρ (Ω m), of an electrical current I (A) injected using two surface electrodes A (injected current I) and B (injected current I). We measure the potential drop ΔV between the electrodes M and N (see Figure 1). The expression of the apparent resistivity is thus the following:

$$\rho = G \frac{\Delta V}{I}. \quad (1)$$

G (1/m) is the geometric factor. Assuming that the medium is semi-infinite (general case study for the soil), G depends only on the distance between electrodes. For a Wenner probe, these distances are: $AM = MN = NB = a$, thus $G = 2\pi a$. In this experiment, a (mm) is equal to $n \cdot s$ where n is the investigation level and s the space between two

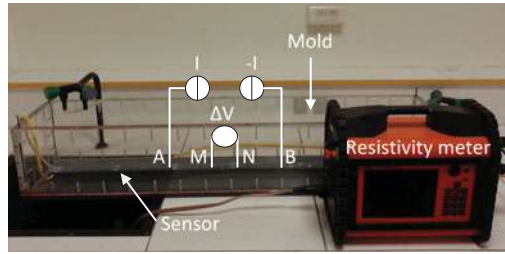


Figure 1. Experimental device and principle of the resistivity measurement.

electrodes (25 mm). If the medium is not semi-infinite (case study of a concrete slab, beam or wall), G depends also on the specimen geometry. In such a case, it has to be evaluated numerically or experimentally. Here, it has been computed thanks to a finite element simulation using the software COMSOL[®].

When the medium is no longer homogeneous the measured resistivities computed using formula (1) are called apparent resistivities. After the surface potentials are measured, the geometric factor is applied to calculate the apparent resistivity for each of the measurement point following the procedure described in [7]. By implementing a large number of four electrodes arrays, we obtain a pseudosection of the subsurface apparent resistivities as shown in Figure 2(a). However they do not directly give the true resistivity distribution of the medium. It must be inverted using an optimisation protocol to find a representative model of the subsurface. These apparent resistivities are then inverted using the commercial code RES2Dinv,[14] to resolve the ‘true’ or inverted resistivity values as a function of depth for a non-homogeneous medium. A section of inverted resistivity is shown in Figure 2(b).

2.2 Material and methods for the measurement of resistivity in concrete using an embedded sensor

2.2.1 The sensor

The sensor used here to perform measurement in concrete (see Sections 4.3 and 5) is a PVC bar equipped with 43 electrodes spaced 25 mm. For the optimisation of the protocol (see Section 4.2) a different model of the sensor was used. It is in fact a prototype of the sensor previously described. It is shorter and equipped with only 32 electrodes spaced

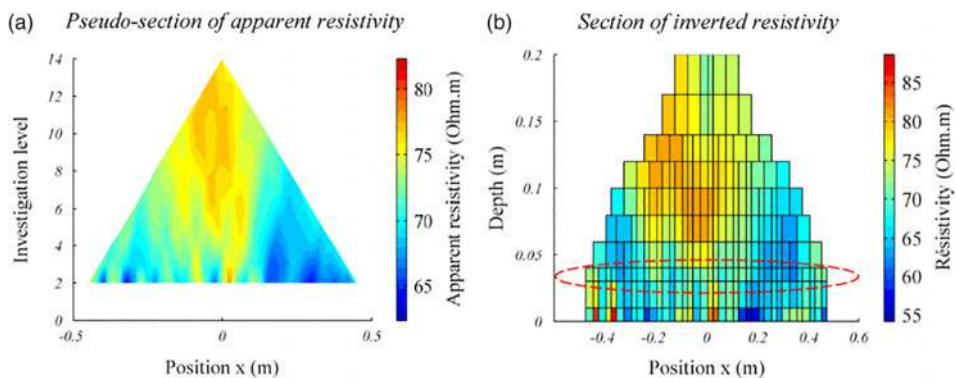


Figure 2. Sample of apparent and inverted resistivity results in concrete.

25 mm. A sketch of the 43 electrodes sensor is given in Figure 3.

The electrodes used in water (optimisation phase of the protocol) are concrete nails of 2.4 mm diameter made of stainless steel while those used in concrete are stainless steel M2.5 screws. The extremity of the nails and screws are cut straight.

In both measurements performed (in water and in concrete), all the outer surface of the electrode is considered to be in contact with the measurement medium. The length of the electrode in water and concrete is set to 5 mm in both cases.

2.2.2 The mold

The bar is placed inside the mold of the beam before the concrete was poured. The beams have sections of 200 mm × 200 mm and measure 1170 mm in total length (see Figure 1).

2.2.3 Wenner array and resistivity measuring cycle timing definition

The electrodes are connected to a device of soil resistivity measurement: the resistivity meter system ABEM Terrameter LS. The electrical sketch of measuring circuit of a previous version of this device can be found in [15]. The 43 or 32 electrodes of the sensors are tested with a Wenner sequence of measurement. The Wenner array is given in Figure 4.

For resistivity measurement the measuring cycle consists of a positive, a double negative and again a positive current pulse (see Figure 5). By averaging the measured voltages all zero shift and linear drift during the measuring cycle is eliminated (source [16]).

The following parameter definitions are used:

- Delay time (T_d). It is defined as the delay from current turn-on until measuring starts (here 200 ms).
- Acquisition time also called integration time (T_i).

3. Quantification and performance objectives of a resistivity sensor embedded in concrete

The sensor developed here is of newly designed with new quantification objectives. Moreover, we aim at assessing uncertainties for future studies about spatial variability assessment and structural health monitoring (SHM) optimisation. Consequently, the

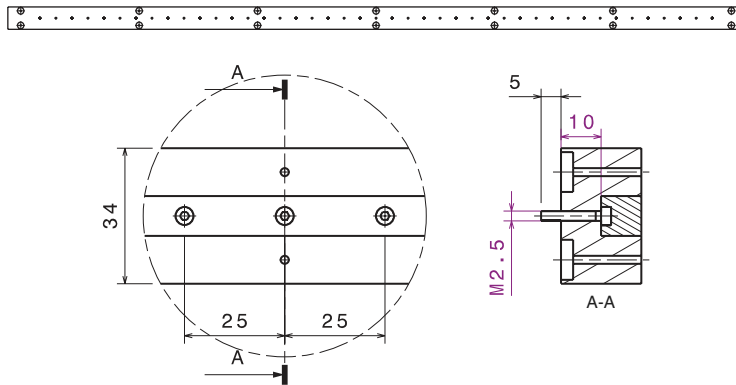


Figure 3. Sketch of the 43 electrodes sensor.

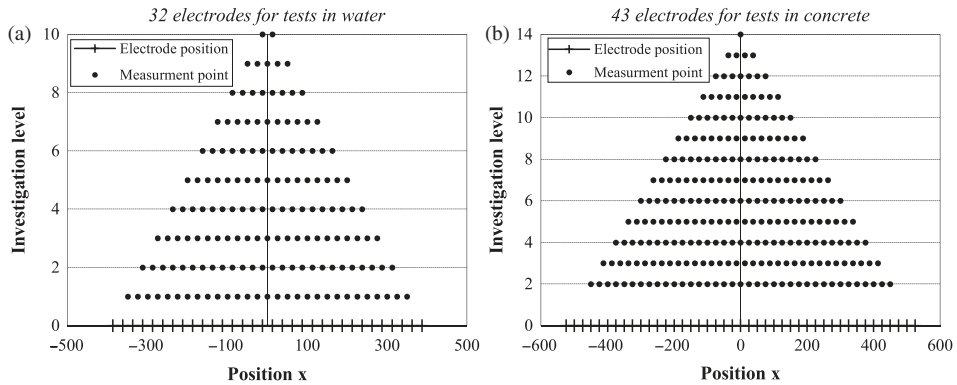


Figure 4. Wenner array for the two versions of the sensor.

sources of uncertainties have to be identified and quantified. In order to deliver quantitative management decision support, we have to define the measurement error. Indeed it is the source of future diagnostic errors.[11,17,18] The uncertainties are traditionally classified into two categories: inherent uncertainties and epistemic uncertainties. The first category consists of hazardous material characteristics (concrete heterogeneity) while the second category consists of the measurement errors, the modelling errors (from the numerical inversion process) and the human factors to name

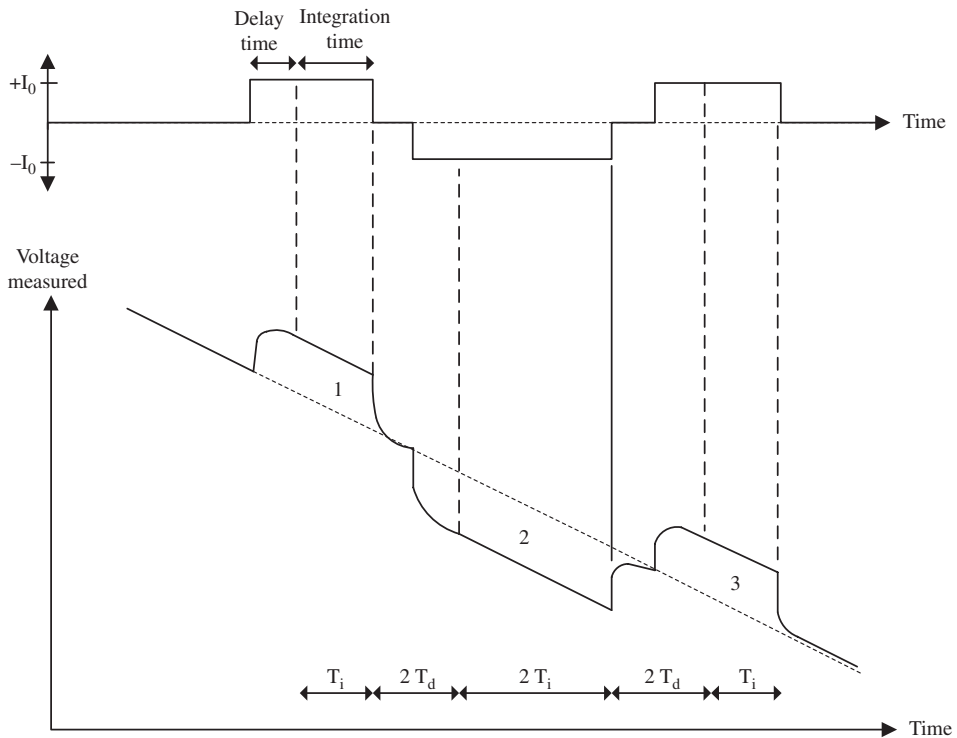


Figure 5. Resistivity measuring cycle timing definition (see [16]).

just a few. Unlike material heterogeneities, the epistemic uncertainties can be reduced with time thanks to knowledge improvement and the modification of measurement procedures regarding concrete.

In this study, we have chosen to explore uncertainties by breaking down the experimental process into two measurement protocols.

First, we performed measurements in a homogenous material assumed to be perfect (low uncertainty on the resistivity) as presented in Section 4. With the repeatability tests, we are able to assess the epistemic uncertainties: the quality of the implementation (sensor implementation), the quality of the electrical contacts, the performances of the acquisition device (measurement accuracy of the electrical currents and potentials) and the manufacturing quality of the sensor (distance between electrodes, electrodes length and parallelism). Via the enquiry of all the measurement levels, we assess the evolution of the uncertainties with the measurement level (or the distance between electrodes). This error is the threshold value for the uncertainties assessed in the second measurement procedure.

We then performed measurement in concretes containing chloride ions. A comparison is done with a concrete without chlorides (reference state). Repeatability tests are made in order to assess the measurement error and to compute an optimal detection threshold for various chloride contents. The kinetic of the concrete hydration is assumed to not be affected significantly by the chloride content in the mixing water. Because all the specimens (concrete beams) are in the same environmental conditions, the resistivity change on a given day are due to differences of chloride content in the mixing water. The tests are performed at different dates after concrete casting: the variation of the material properties and the degree of hydration are integrated within the evaluation of uncertainties.

4. Performances assessment and optimisation of the acquisition system (tests in water)

Before performing tests in concrete, we have worked in a medium of known and homogenous resistivity in order to estimate the measurement reliability and the standard error of the entire acquisition system (sensor and Terrameter) in case of a reference material without spatial variability. The mold built for the concrete was instrumented with the resistivity sensor and then filled with water at a constant temperature of 20°C. The resistivity of water was monitored using a conductivity cell. Then the pseudosection of apparent resistivities obtained with the Terrameter allows computation of the dispersion of resistivity values due to the acquisition system itself. We perform 10 repeatability tests for each measurement point $M(x_i, y_i)$ (Figure 2(a)). Then different quantities are computed in view to optimise the protocol on one hand and assess and model the error for the optimised protocol (see Section 4.3) on the other.

For the level featuring the highest number of points, and thus studied for limitation of the statistical bias, we seek to analyse the correlation between the measurement error, computed as the standard deviation (SD) of the sample containing the 10 values of the repeatability test $\tilde{v}_j(x_i, y_i)$, $j \in \{1; \dots; 10\}$ and the magnitude of the value measured at this point and noted $\bar{v}(x_i, y_i)$. This one is defined as the average of the 10 points. The analysis performed here follows the guidelines issued in [19].

If a negligible correlation is shown, it is possible to assume that error is independent of the magnitude and thus to aggregate the errors, level by level. We compute the SD $\{\tilde{v}_j(x_i, y_i) - \bar{v}_j(x_i, y_i)\}$, $(i, j) \in \{1; \dots; n_N\} \times \{1; \dots; 10\}$ where n_N is the number of measuring points of level N . It allows reduction of the statistical error because the number of measuring points for each level is given by the relationship: $n_{N+1} = n_N - 3$.

For each of the 10 repeatability tests, a reference value is given by the conductivity probe $\hat{v}_j(x_i, y_i), j \in \{1; \dots; 10\}$. The bias is computed using the relationship: $b_{j,k} = \hat{v}_j - \bar{v}_{j,k}$ where $\bar{v}_{j,k}$ is the mean value for the level k and for the test j .

4.2 Optimisation of the protocol: settings of the resistivity device

In this section, we have used a version of the resistivity sensor composed of 32 electrodes instead of 43 for the sensors used in concrete. This smaller probe allows to perform tests quickly but does not impact the conclusions about the best measurement settings. With the small sensor 155 measurements points were recorded instead of 247 in the final protocol.

The geometry of the probe being fixed, two parameters are selected for optimising the protocol: the duration and the intensity of injection. Their effect should be quantified in view to select the best couple of these parameters. Our criterion is the reduction of the SD during the repeatability tests. We perform the optimisation tests in water whose electrical resistivity is about $20 \Omega \text{ m}$. It is thus in the same order of magnitude that the electrical resistivity of concrete (see Figure 9) which is in the range $10\text{--}70 \Omega \text{ m}$. Current intensity being more influent, the experimental design is a conditional one. First, the optimal intensity is obtained and then the time of injection is optimised. As defined in Figure 5, the time of injection is the sum of the acquisition time and the delay time. Here the delay time is set to 200 ms.

- first the time of acquisition or integration is set to 0.2 s and only the intensity I is considered as an optimisation parameter taking values in the set $\{0.5; 1; 2; 5; 10\}$ (mA);
- after setting the intensity of injection to the best value according to our criterion, the time T_i of integration is considered as an optimisation parameter taking values in the set $\{0.1; 0.2; 0.5; 1\}$ (s).

Figure 6 plots the result of the first step for the six first levels. It is shown that the effect of current intensity is not linear and the worst protocol is obtained for $I = 1 \text{ mA}$ for which the SD is high (always more than $0.2 \Omega \text{ m}$) while the best results are obtained for current injection of 2 and 5 mA (CoV in average of respectively 0.15% and 0.1%).

Even if an intensity of 5 mA appears as a better choice than an intensity of 2 mA to reduce the SD of measurement performed in water, we made the tests in concrete using an

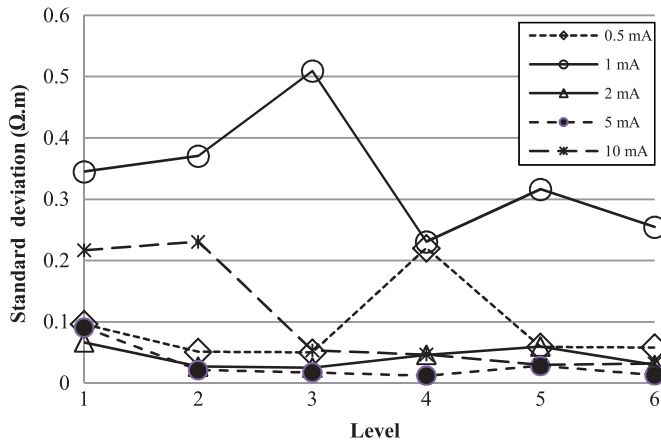


Figure 6. Optimisation of the intensity of injected current (repeatability tests performed in water).

intensity of injected current setting to 2 mA. Indeed, considering the modest difference between the two settings on the SD error, we prefer used the lower intensity for further applications. The aim is to limit the influence of the injected current on the concrete in particular during the first days when chemical reactions could be affected by the magnitude of current intensity.

Let us focus now on the second step of the experimental plan. Figure 7 plots the evolution of the scatter estimate (SD), for the first six levels, changing the duration of current injection. For the lower integration time $T_i = 0.1$ s, the error decreases with the level when the opposite is observed for $T_i = 0.5$ s. The best result is obtained for a duration of acquisition setting to 0.2 s.

In the following we decide to set the current injection parameters to: $T_i = 0.2$ s and $I = 2$ mA with T_i , the time of integration.

4.3 Error assessment and modelling

We now use the full scale probe developed for concrete and assess the measurement error in view to evaluate the relevance of the optimised settings on water.

Following the procedure described in Section 4.1, three analyses are made in order to understand the origin of the measurement error and to model it.

- First we analyse the correlation between the measurement error and the measured value; this analysis is performed for each investigation level.
- Then, we analyse the effect of the distance to the injection electrode; the measurement error is computed for a given investigation level.
- Finally we compute the measurement bias for each level in comparison with the reference value given by a conductivity probe.

We plot in Figure 8(a) the scatter graph obtained for the second level of investigation which contains 37 points and limits statistical bias.

The scatter graph suggests a very fair correlation that we extrapolate to the independence between the value measured and the measurement error. It is thus possible to aggregate the errors, level by level, by centring the difference on the measuring point. Here n_N (the number of measuring points) takes the values 37–13 for the levels 2–10. Ten repeatability

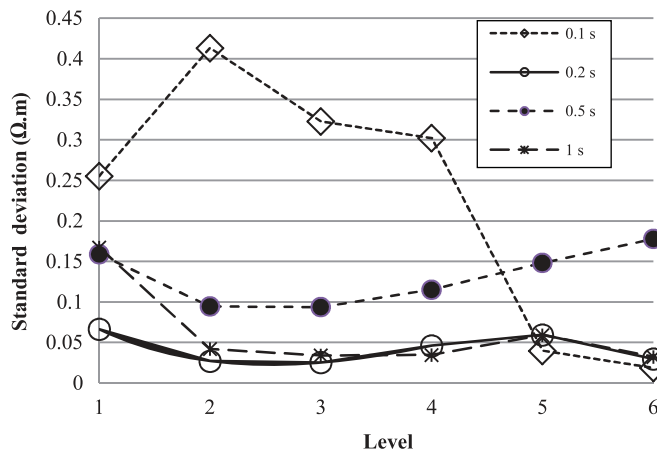


Figure 7. Optimisation of the time of integration T_i (repeatability tests performed in water).

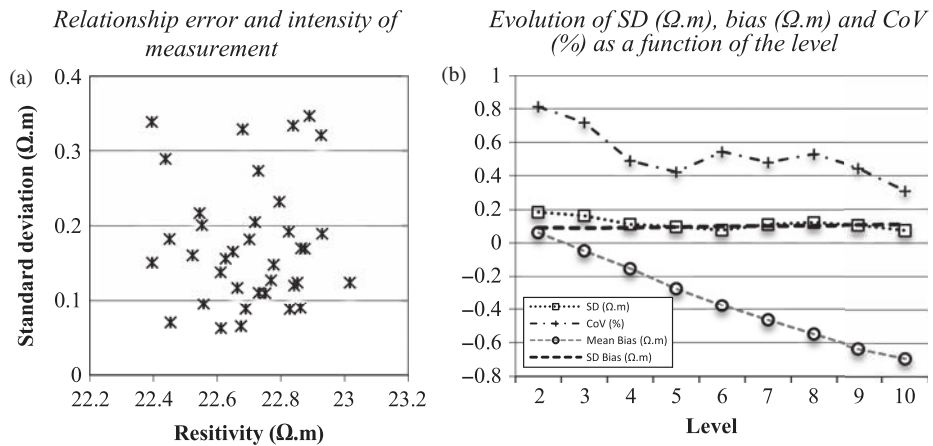


Figure 8. Error assessment (repeatability tests performed in water).

measurements are available and the smallest sample contains 130 values. We plot on Figure 8(b) the evolutions of the SD ($\Omega.m$) and the CoV (%) depending on the level of investigation. The value of the CoV slightly decreases with the level and is around 0.5%.

The values measured using the conductivity probe during all the tests are from 22.66 to 22.88 $\Omega.m$ with a mean value of 22.76 $\Omega.m$. The low influence of the water resistivity or temperature variation is thus present in the data analysed.

The evolution of the average bias and its SD, computed using the results of 10 tests, are plotted in Figure 8(b) as a function of the level. The SD is in the order of 0.1 $\Omega.m$. The bias is low, staying in the range from 0.05 to 0.7 $\Omega.m$. The CoV is therefore negligible because it is in average of 0.5% and it always stays below 0.8%. This confirms the importance to precisely measure a reference value using the conductivity probe for each test. Indeed the variability of the medium, estimated to be around 1%, is by the same order of magnitude as the variability of the protocol measured here.

One can remark that the values of CoV given here are different from those found with the 32 electrodes sensors. We must specify that the shapes of the electrodes are different for the two sensors. The nails are ringed for the 32 electrodes sensors and threaded for the one used in concrete (43 electrodes).

The final conclusion of this study is that we have verified that we have selected a protocol for which the error of measurement is negligible.

5. Evaluation of the measurement sensitivity for the detection of chloride (tests in concrete)

In order to assess the detection threshold of chlorides, we have cast concrete beams, with different contents of chlorides, in instrumented molds. The water–cement ratio of the concrete is equal to 0.7. It is made with a Portland cement CEM I (see Table 1). The composition of the concrete mix is given on Table 2 and its mechanical properties are given in [20]. Chloride ions were dissolved in the mixing water before the introduction in the mixer. A portion of these ions is bound to the cement paste while the remaining chlorides are free and are therefore found in pore water. These free ions are detectable using resistivity measurement. It is an interesting property for the SHM because only free ions may be able to migrate to the concrete reinforcements, locally decrease the pH, leading to the corrosion.

Table 1. Chemical composition of the cement.

<i>Compounds</i>	<i>Mass (%)</i>
CaO	64.95
SiO ₂	21.25
Al ₂ O ₃	3.47
Fe ₂ O ₃	4.23
MgO	0.96
K ₂ O	0.28
Na ₂ O	0.10
SO ₃	2.63
Specific surface (m ² /Kg)	382
Density	3.18
<i>Main compounds (Bogue's composition)</i>	
C ₃ S	67.5
C ₂ S	10.7
C ₃ A	2.64
C ₄ AF	12.8
Gypsum	3.3

At the end of the experiment, some cores were extracted from beams to determine the chloride content into concrete. Cylindrical cores were ground using a grinding instrument to get enough concrete powder. The total and free chloride contents were determined following the procedure recommended by the RILEM Technical Committee 178-TMC [21]. The correspondence between the chloride content in the concrete and the initial chloride content in the mixing water is given in Table 3. It is shown that increasing the chloride content in the mixing water increases mainly the free chloride content.

The beams instrumented with the resistivity sensors were stored in a climatic chamber with maintained temperature (20°C) and relative humidity (85%). The resistivity measurements were performed at times 1, 7, 14, 21, 28, 85 and 118 days after pouring of concrete. The evolution of the resistivity as a function of the time for the four chloride contents are plotted in Figure 9 for the level 3. Note that the error bars depict the SD of all 'inverted' resistivity values for the level 3 (see the area circled in red on the Figure 2(b)) where reinforcing bars could be placed. The material is supposed to be homogenous (mastered manufacturing processes in laboratory and phenomenon of segregation negligible at this scale). The SD error for all of the resistivity values, measured in a same beam, is in the order of 10% of the mean resistivity which can be considered to be low. This curve shows a significant increase of the resistivity during the first days of the concrete life. For the first two days, the increase is related to the setting time and then the hardening of the concrete leading to a reduction of the porosity. It is the major

Table 2. Concrete mix composition.

<i>Compounds</i>	<i>Mix ingredients (kg/m³)</i>
Coarse aggregate (12–20 mm)	563.4
Medium aggregate (4–12 mm)	433.7
Sand (Boulonnais) (0–4 mm)	903.5
Cement CEM I 52.5 N PM ES	260
Total water	182
Water to binder ratio (W/B)	0.7

Table 3. Correspondence between the free chloride content in the concrete and the initial chloride content in the mixing water.

	<i>Chloride content in mixing water (g/l)</i>	<i>Free chloride content (g/g of concrete)</i>	<i>Total chloride content (g/g of concrete)</i>
Beam 1	0		
Beam 2	30	0.00096	0.00169
Beam 3	60	0.00159	0.00238
Beam 4	120	0.00319	0.00344

phenomenon inducing an increase of the resistivity. At 90 days, the material has nearly reached its maximum strength. After 90 days, the water remaining not consumed by the chemical reactions starts to evaporate leading to the drying out of the porous space. With time, the increase of resistivity becomes weak but stays significant.

Another interesting behaviour is that the resistivity does not vary linearly with the chloride content in the mixing water. For instance at 118 days, it reaches 50, 46 and 32 Ω m for concentrations of 30, 60 and 120 g/l respectively. But when focusing on the free chlorides content (see Table 3), Figure 10 shows that the evolution is linear at the end of the experiment. It confirms that the resistivity is a robust indicator for free chloride assessment.

Presuel-Moreno et al. [22] made similar resistivity measurements with four electrodes equi-spaced as per the Wenner arrangement on cylindrical concrete specimens prepared with ordinary Portland cement (OPC) and a water–cement ratio of 0.4. The evolution versus time for specimen exposed in fog room after demoulding was quantified until 1300 days (3.5 years). The resistivity value increased at a quick rate during the first 30 days and then increased at a slow rate. The shapes of resistivity evolution versus time plotted in Figure 9 show very similar trends for all of the specimens and these evolutions are similar to those obtained by Presuel Moreno for OPC concrete specimens. This was related to the evolution of the concrete microstructure. Lübeck et al. [23] found the same results with concrete specimen prepared with OPC and a water–cement ratio of 0.55 stored in a wet chamber after demoulding. The electrical resistivity measured using the Wenner’s method increased from 100 Ω m at 3 days to 350 Ω m at 91 days and the resistivity was almost (330 Ω m) constant between 56 days and 91 days.

5.1 Repeatability tests performed in concrete

We consider first the repeatability tests using the protocol presented in Section 4.3. The main difference is that the true value of resistivity inside the concrete cannot be assessed and consequently, the bias is not computed. The objective of the experiment is to confirm the good repeatability highlighted with the tests in water. We conducted five tests for each measurement point $M(x_i, y_i)$ (points on the Figure 2(a)), at day 118 on the concrete beam poured without chlorides. Then we performed the same analysis as explained in the case of water for the steps (a) and (b) described in the Section 4.3. Nevertheless, in this analysis, the numerical error resulting from the inversion process appears.

We plot on Figure 11(a) the scatter graph for level 2. It suggests a very fair correlation between the measurement error and the mean value measured at each point. This result is the same at all levels. Consequently we assume that the measurement error is independent of the intensity of the measure. It is thus possible to aggregate the errors for each level.

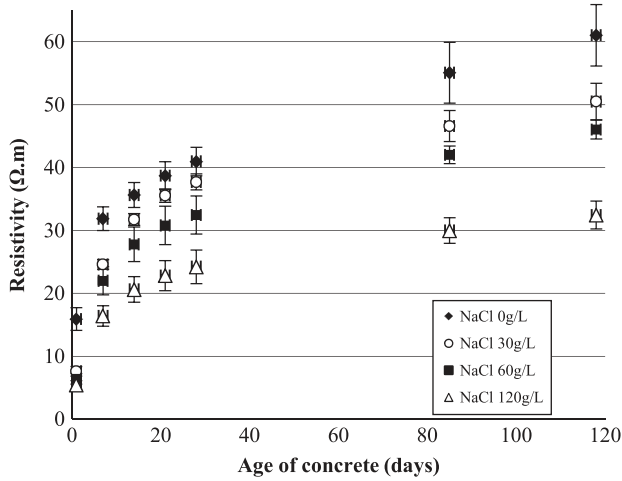


Figure 9. Monitoring of the hydration in a concrete made with a Portland cement CEM I (water-cement ratio = 0.7) containing different contents of chlorides in the mixing water.

We plot on Figure 11(b) the SD (Ωm) and the COV (%) evolution as a function of the level. We notice that the SD is constant and the CoV not changes much. With a COV of 0.1%, two conclusions are inescapable: we can neglect the repeatability error and in the subsequent stages of the study, no repeatability tests are needed.

5.2 Evaluation of the chloride detection threshold

In order to determine the detection threshold of chlorides, we study a given measurement level. We focus on an intermediary level to avoid surface phenomena that are not of interest in the context of the evaluation of the chloride penetration near concrete reinforcement. An additional constraint is to have enough points to obtain a good

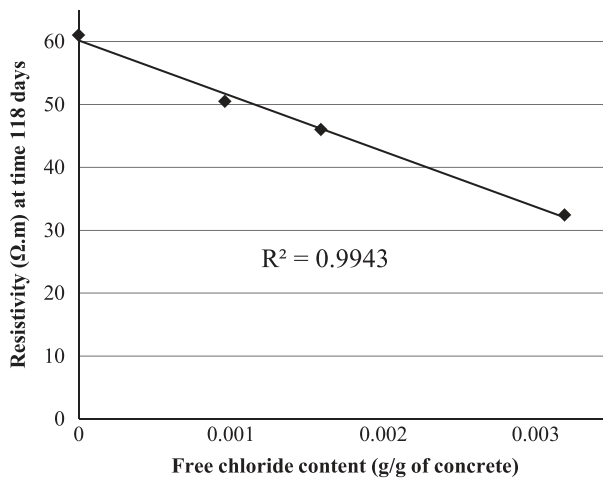


Figure 10. Relation between resistivity and free chloride content: evaluation of the regression coefficient.

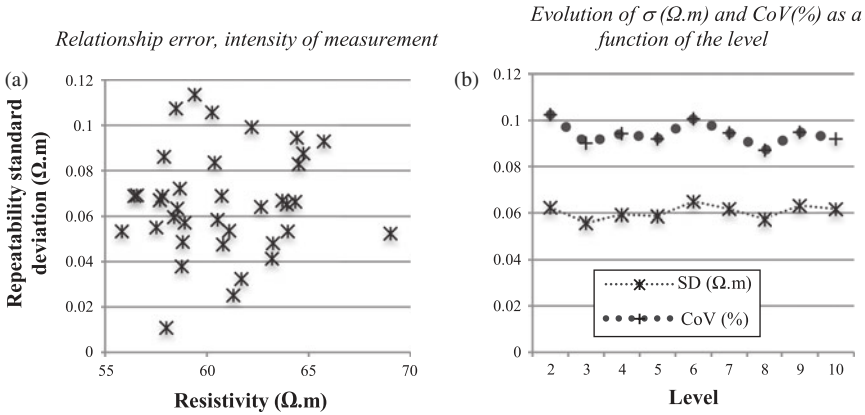


Figure 11. Repeatability tests performed on concrete (without chloride in mixing water).

statistical assessment of the material variability. Thus we choose the level 3 containing 37 elements for which the resistivity is computed during the inversion process. This level corresponds to a depth of investigation approximately equal to 35 mm (see the area circled in red on the Figure 2(b)). In the context of the SHM, it could be the position of concrete reinforcements.

As we can see in Figure 9, the higher the chloride level is, the easier it is to detect chlorides with a resistivity measurement device at a given point in time. This article attempts to quantify the detection capability at a given point in time as a function of the chloride content. The temporal evolution allows us to analyse the influence of the open porosity that decreases over time. First of all, we will determine the optimal detection threshold and then the optimal probability of detection (PoD) as a function of the chloride content at different dates. To this end, we use a probabilistic approach to define the quantities ‘PoD’ and ‘probability of false alarm’ (PFA). We use the same definition as proposed in a previous study of void detection within tendon ducts.[24] The ‘noise’ here consists of the concrete without chlorides for which no detection of chlorides should occur. We seek to detect a defect (here the presence of chloride in concrete) compared with a material without defects. The resistivity of a concrete without chlorides is higher than the resistivity of the same concrete containing chlorides. Thus the distribution of the signals ‘resistivity noise’ and ‘resistivity signal + noise’ are reversed from the definitions usually applied.[19] The probability to detect the random defect (measured defect) \hat{d} and the PFA are then given by:

$$\text{PoD} = \int_{-\infty}^{a_d} f_{SN}(\hat{d})\delta\hat{d}, \quad \text{PFA} = \int_{-\infty}^{a_d} f_N(\eta)\delta\eta, \quad (2)$$

where a_d is the detection threshold. Below this value, no defects are detectable. f_{SN} and f_N are respectively the probability density functions of the ‘signal + noise’ and the ‘noise’. We choose to define the detection threshold using the ROC curve that links the points of coordinates [PFA; PoD]. Each point corresponds to measurements performed using different parameters that affect it (for example, the settings, the sensor manufacturing, the device for current injection...). The curve plotted in Figure 12(b) is obtained by continuously varying the parameter a_d . According to the $\alpha\delta$ method, we find the optimal

detection threshold that minimises the distance δ between the corresponding point of the ROC curve and the best performance point at coordinates [0; 1] (see [24]).

We plot the ROC curves and apply the method to a concrete at 28 days for the investigation level 3. To determine the detection threshold, we use the most unfavourable configuration i.e. the concrete containing the lower chloride content (30 g/l) in the mixing water (this value is close to the sea water content). The resistivity distribution for the ‘noise’ (0 g/l) and the ‘signal + noise’ (30 g/l) are plotted in Figure 12(a). In order to fit the distribution of resistivity, we have tested three classical distributions: a normal distribution, a generalised extreme values (GEVs) distribution and a student distribution according to previous works.[19] To find the best one, we implement the maximum-likelihood method [by using the maximum of the log(likelihood) estimate (MLE)]. The three parameters distribution GEV gives the best MLE and fits well the asymmetry of signal. Then we plot the experimental ROC curves (obtained by numerical integration of Equation (2) using an increment of 0.2) and the ROC curves obtained by fitting the distributions. We observe a good agreement between the ROC curves except in the central area where the fitting of the noise distribution is not totally satisfactory (see Figure 12(a)). Then we compute the detection threshold a_d corresponding to the lowest measurement δ . The line segment is plotted in red. We thus obtained $\delta = 0.2$, and $a_d = 37.85 \Omega \text{ m}$. The value of δ , in the range $[0, \sqrt{2}/2]$ can be considered low in risk analysis.[12] The point of optimal detection has coordinates: [0.14; 85.5] and the probability of optimal detection is 85.5%.

Let us now consider the detection reliability after 85 days. The Figure 9 shows that the difference between the resistivity for 0 and 30 g/l increases both in main trend and scatter. The δ measure is very efficient for analysing the performance in this configuration. The value of δ falls from 0.2 at 28 days to 0.0026 at 85 days, showing a strong improvement of detection reliability. The corresponding detection threshold moves from 37.85 to 46.55 $\Omega \text{ m}$ because the main trend of resistivity increases with time and PoD reaches 0.999 when PFA falls to 0.002. Finally, the reliability of a nondestructive testing (NDT) tool or sensor is generally expressed in terms of PoD curve: this curve connects the PoD values when the defect increases.[17,25] Here the defect is the chloride content that increases from 30 to 120 g/l. The Figure 13 plots the PoD curve at 28 and 85 days for the previous detection threshold. It is shown that the PoD is increasing with the defect and that the slope of the PoD curve at 85 days is higher. That is due to the better reliability of chloride detection after 85 days.

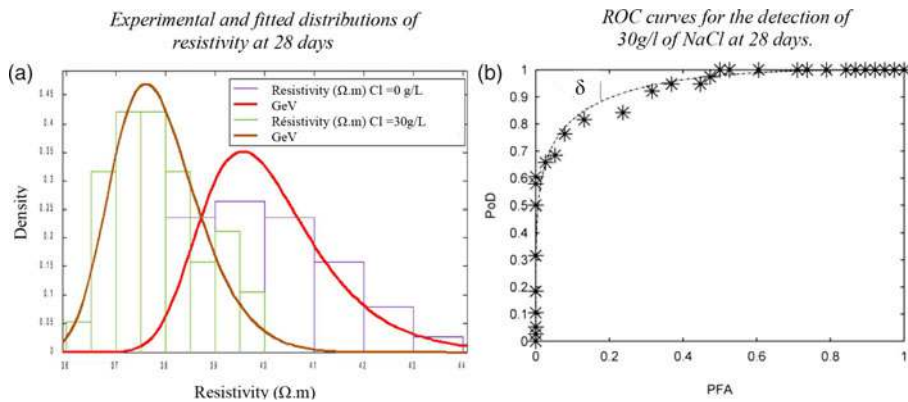


Figure 12. Evaluation of the chloride detection threshold (28 days).

6. Conclusion

This paper aims to evaluate and optimise the performance of chloride ions detection sensor integrated, based on the measuring of the DC electrical resistivity and quantify some relationships between chlorides in concrete and resistivity. The major issue in resistivity measurements performed in concrete is the dispersion of results mainly linked to the material heterogeneity and electrical contact limitations. To take into account these uncertainties, we used a measurement device based on Geoelectrical Imaging methods and proposed a resistivity sensor of newly designed. It can be embedded in concrete for in-situ measurements and it gives richer information than the one delivered by conventional resistivity measurement sensors. Thus, it allows the use of statistical analysis and quality assessment methods.

We then provide a complete protocol for assessing uncertainties when measuring change of properties by using embedded sensors. It has the following advantages:

- analyses and optimises the performances of the acquisition system through repeatability tests and by calibration of the resistivity measurement device in a homogeneous environment of known resistivity;
- uses this optimal configuration on the assessment of uncertainties when measuring resistivity in a concrete;
- qualifies the sensitivity of the resistivity to chloride content in the mixing water and to the content of free chlorides in the concrete;
- quantifies the interest of the device and the protocol by considering destructive test to link resistivity to free chlorides;
- measures the concrete resistivity evolution for four contents of chloride ions in mixing water: 0, 30, 60 and 120 g/l respectively, up to 120 days from casting;
- determines the optimal detection threshold by plotting the ROC curves from the resistivity distribution for the ‘noise’ (concrete without chlorides) and the ‘signal + noise’ (concrete containing chlorides);
- finally provides an optimal detection threshold and then the optimal PoD as a function of the chloride content and the time.

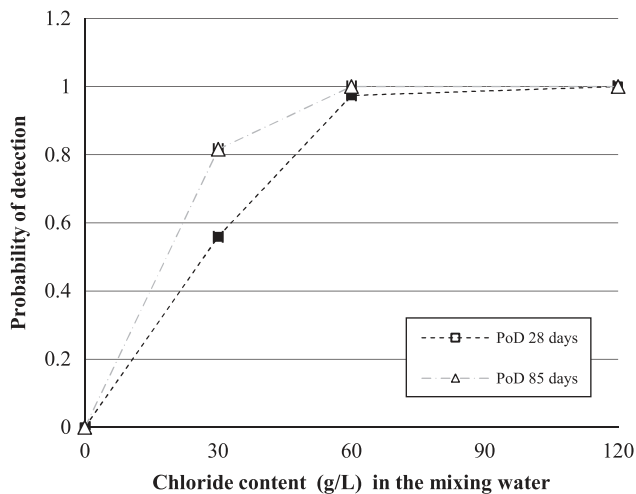


Figure 13. Evolution of the PoD between 28 and 85 days.

Thanks to a statistical analysis of uncertainties and a probabilistic modelling, we have assessed a detection threshold of $37.85 \Omega \text{ m}$ as a compromise between the PoD and the PFA: the probability to detect chloride content in concrete at 28 days higher than 30 g/l is then 85.5% . This work offers promising prospects on the recommendation of a detection threshold as a function of time. We could also establish a unique threshold in order to optimise the SHM as a function of time: this question appears to be relevant in this paper because the optimal detection threshold is shown to be time dependent (during the first 85 days) for a given chloride level assessment (30 g/l in the mixing water). Another prospect is to perform such analysis in a realistic situation i.e. with a chloride gradient in a concrete and a stochastic variability of the resistivity.

Disclosure statement

No potential conflict of interest was reported by the authors.

References

- [1] Torres-Luque M, Bastidas-Arteaga E, Schoefs F, Sanchez-Silva M, Osma JF. Non-destructive methods for measuring chloride ingress into concrete: state-of-the-art and future challenges. *Constr Build Mater.* 2014;68:68–81.
- [2] Saleem M, Shameem M, Hussain SE, Maslehuddin M. Effect of moisture, chloride and sulphate contamination on the electrical resistivity of portland cement concrete. *Constr Build Mater.* 1996;10(3):209–214.
- [3] Polder RB. Test methods for on-site measurement of resistivity of concrete a {RILEM} TC-154 technical recommendation. *Constr Build Mater.* 2001;15(23):125–131.
- [4] Polder RB, Peelen WHA. Characterisation of chloride transport and reinforcement corrosion in concrete under cyclic wetting and drying by electrical resistivity. *Cem Concr Compos.* 2002;24(5):427–435.
- [5] Hornbostel K, Larsen CK, Geiker MR. Relationship between concrete resistivity and corrosion rate a literature review. *Cem Concr Compos.* 2013;39:60–72.
- [6] McCarter W, Chrisp T, Starrs G, Adamson A, Owens E, Basheer P, Nanukuttan S, Srinivasan S, Holmes N. Developments in performance monitoring of concrete exposed to extreme environments. *J Infrastruct Syst.* 2012;18(3):167–175.
- [7] du Plooy R, Palma Lopes S, Villain G, Derobert X. Development of a multi-ring resistivity cell and multi-electrode resistivity probe for investigation of cover concrete condition. *NDT & E Int.* 2013;54:27–36.
- [8] Lataste JF, De Larrard T, Benboudjema F, Semenadisse J. Study of electrical resistivity: variability assessment on two concretes: protocol study in laboratory and assessment on site. *Eur J Environ Civil Eng.* 2012;16(3–4):298–310.
- [9] Giraldo DF, Dyke SJ, Caicedo JM. Damage detection accommodating varying environmental conditions. *Struct Health Monit.* 2006;5(2):155–172.
- [10] Salta S, Schoefs M, Ricardo F, Chaplain J, Breyse M, Yotte D. Accounting for variability and uncertainties in NDT condition assessment of corroded RC-structures. *Eur J Environ Civil Eng.* 2009;13(5):573–591.
- [11] Bastidas-Arteaga A, Schoefs F. Stochastic improvement of inspection and maintenance of corroding reinforced concrete structures placed in unsaturated environments. *Eng Struct.* 2012;41:50–62.
- [12] Schoefs F, Boero J, Clement A, Capra B. The alpha delta method for modelling expert judgement and combination of non-destructive testing tools in risk-based inspection context: application to marine structures. *Struct Infrastruct Eng.* 2012;8(6):531–543.
- [13] Khan AA, Vrabie V, Beck YL, Mars JI, D’Urso G. Monitoring and early detection of internal erosion: distributed sensing and processing. *Struct Health Monit.* 2014;13:562–576. First published on May 20, 2014.
- [14] Loke MH, Barker RD. Rapid least-squares inversion of apparent resistivity pseudosections by a quasi-newton method. *Geophys Prospect.* 1996;44(1):131–152.

- [15] ABEM. SAS 300 instruction manual. 2010. <http://www.abem.se/software.php>
- [16] ABEM. User guide Terrameter LS. 2012. <http://www.abem.se/software.php>
- [17] Rouhan A, Schoefs F. Probabilistic modeling of inspection results for offshore structures. *Struct Saf.* 2003;25(4):379–399.
- [18] Sheils E, O'Connor A, Schoefs F, Breysse D. Investigation of the effect of the quality of inspection techniques on the optimal inspection interval for structures. *Struct Infrastruct Eng.* 2012;8(6):557–568.
- [19] Schoefs F, Clement A, Nouy A. Assessment of {ROC} curves for inspection of random fields. *Struct Saf.* 2009;31(5):409–419.
- [20] Fraj AB, Bonnet S, Khelidj A. New approach for coupled chloride/moisture transport in non-saturated concrete with and without slag. *Constr Build Mater.* 2012;35:761–771.
- [21] RILEM TC 178-TMC. Analysis of total chloride content in concrete. *Mater Struct.* 2002;35(9):583–585.
- [22] Presuel-Moreno F, Wu Y-Y, Liu Y. Effect of curing regime on concrete resistivity and aging factor over time. *Constr Build Mater.* 2013;48:874–882.
- [23] Lübeck A, Gastaldini ALG, Barin DS, Siqueira HC. Compressive strength and electrical properties of concrete with white Portland cement and blast-furnace slag. *Cem Concr Compos.* 2012;34(3):392–399.
- [24] Schoefs F, Abraham O, Popovics JS. Quantitative evaluation of contactless impact echo for non-destructive assessment of void detection within tendon ducts. *Constr Build Mater.* 2012;37:885–892. *Non Destructive Techniques for Assessment of Concrete.*
- [25] Frangopol D, Tsompanakis Y. *Maintenance and safety of aging infrastructure.* Edited by Dan Frangopol and Yiannis Tsompanakis. CRC Press; 2014.